

High-temperature intrinsic ferromagnetism in heavily Fe-doped GaAs layers

A.V. Kudrin^{1*}, V.P. Lesnikov¹, Yu.A. Danilov¹, M.V. Dorokhin¹, O.V. Vikhrova¹, P.B. Demina¹, D.A. Pavlov¹, Yu.V. Usov¹, V.E. Milin¹, Yu.M. Kuznetsov¹, R.N. Kriukov¹, A.A. Konakov¹ and M.P. Temiryazeva²

¹Lobachevsky State University of Nizhny Novgorod, Gagarin av. 23/3, 603950 Nizhny Novgorod, Russia

²Kotel'nikov Institute of Radioengineering and Electronics of RAS, Fryazino Branch, 141190 Fryazino, Russia

*kudrin@nifti.unn.ru

The layers of a high-temperature novel (Ga,Fe)As diluted magnetic semiconductor (DMS) with an average Fe content up to 17 at. % were grown on (001) *i*-GaAs substrates using a pulsed laser deposition in a vacuum. The transmission electron microscopy investigations revealed that the layers are epitaxial, do not contain any second-phase inclusions, but contain the columnar regions of overlapped microtwins. The *n*-type conductivity of the obtained (Ga,Fe)As layers is apparently associated with the formation of a Fe impurity band within the GaAs band gap. A hysteretic negative magnetoresistance was observed in the layers up to room temperature. Magnetoresistance measurements point to the out-of-plane magnetic anisotropy of the (Ga,Fe)As layers related to the presence of the columnar regions. The studies of the magnetic circular dichroism confirm that the layers are intrinsic ferromagnetic semiconductors with the Curie point up to at least room temperature. It was suggested that in heavily Fe-doped GaAs layers the ferromagnetism is related to the Zener double exchange between Fe atoms with different valence states (Fe³⁺ and Fe²⁺) via an intermediate As atom.

1. Introduction

Heavily Fe-doped diluted magnetic semiconductors (DMS) are considered as promising materials for semiconductor spintronics since the recent synthesis of the (Ga,Fe)Sb [1-4] and (In,Fe)Sb [5,6] DMSs with a Fe content up to 17 at. % and above-room temperature (RT) Curie point. At present, the nature of ferromagnetism in Fe doped narrow-gap ((In,Fe)As, (Ga,Fe)Sb, (In,Fe)Sb) and wide-gap III-V ((Al,Fe)Sb) semiconductors is a subject of research. Apparently the ferromagnetism in (III,Fe)V DMSs is not carrier-mediated but related to some superexchange interaction between Fe atoms [5-8]. In particular, we recently observed a remarkably weak interrelation between the ferromagnetism and the charge carrier concentration in (In,Fe)Sb that is fundamentally different from Mn doped III-V DMSs [9]. Obtained results raise the question of creating the ferromagnetic layers of a practically important GaAs semiconductor by introducing a large amount of Fe atoms (> 10 at. %) during an epitaxial growth.

There are a few papers from the early 2000s about the formation of the (Ga,Fe)As layers by molecular beam epitaxy (MBE) with a relatively low Fe content (up to 3.5 at. %). In [10-12] the Ga_{1-x}Fe_xAs layers with *x* in the range of 0.007 – 0.07 were grown at the temperatures in the range of 260 – 580°C. These layers were high-resistive with a weak *n*-type conductivity. The structures obtained at 260 °C were characterized as Ga_{1-x}Fe_xAs homogeneous paramagnetic epilayers, whereas the structures obtained at 350 – 580 °C were GaAs epilayers with second-phase ferromagnetic inclusions. These (Ga,Fe)As layers were obtained at the relatively high temperatures and contained the relatively low amount of iron. Since by now both conductive ((In,Fe)As, (Ga,Fe)Sb, (In,Fe)Sb)) and insulating ((Al,Fe)Sb) ferromagnetic (III,Fe)V DMSs have been obtained, it

can be expected that the synthesis of ferromagnetic (Ga,Fe)As is also possible.

In this work we present the results of investigations of conductive (Ga,Fe)As layers with the ferromagnetic properties up to room temperature.

2. Experiments

The GaAs and (Ga,Fe)As layers were grown by a pulsed laser deposition (PLD) in a vacuum on semi-insulating (001) GaAs substrates [5,9,13]. The Fe content was set by the technological parameter $Y_{Fe} = t_{Fe}/(t_{Fe} + t_{GaAs})$, where t_{Fe} and t_{GaAs} are the ablation times of the Fe and GaAs targets, respectively.

The surface of the structures was examined by atomic force microscopy (AFM), magnetic force microscopy (MFM) and Kelvin probe force microscopy. The structural properties of the samples were investigated by an analytical transmission electron microscopy (TEM). The distribution of constituent elements was obtained by an energy-dispersive X-ray spectroscopy (EDS) during microscopy investigations. Optical reflectivity spectra were obtained at RT in the spectral range of 2.4 – 6 eV. The *dc* magnetotransport measurements were carried out in the van der Pauw and Hall bar geometry in a closed-cycle He cryostat. The investigations of the magnetic circular dichroism (MCD) were performed in the cryostat in the spectral range from 1.37 to 2.03 eV using a monochromatized emission of a xenon arc lamp as a light source.

In this study we present results for the following structures: an undoped GaAs layer grown at 200 °C (sample 200-0, grown by the sputtering of the GaAs target only), three (Ga,Fe)As layers with $Y_{Fe} = 0.08$, $Y_{Fe} = 0.17$, $Y_{Fe} = 0.25$ grown at $T_g = 200$ °C (samples 200-8, 200-17 and 200-25, respectively) and a (Ga,Fe)As layer with $Y_{Fe} = 0.25$ grown at 180 °C (a

sample 180-25). The technological thickness of the (Ga,Fe)As layers was ~ 40 nm.

3. Results

3.1. Structural and optical properties

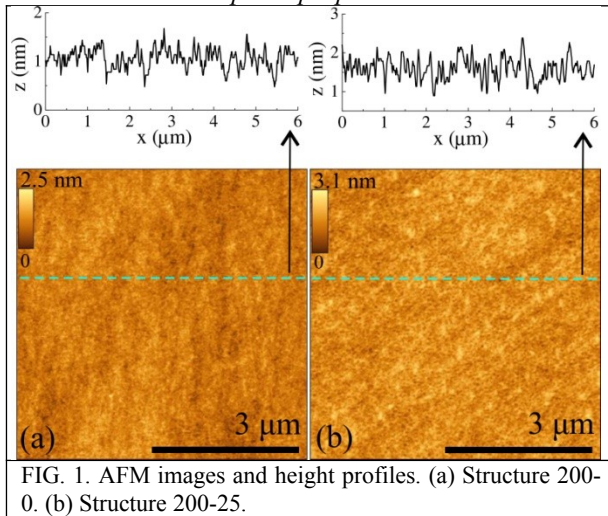


FIG. 1. AFM images and height profiles. (a) Structure 200-0. (b) Structure 200-25.

Figure 1 shows the AFM surface morphology of the structures 200-0 (Figure 1(a)) and 200-25 (Figure 1(b)). All obtained (Ga,Fe)As layers (and the GaAs layer) have the smooth surface with a root mean square (RMS) roughness of about 0.3 nm.

Figure 2(a) shows the overview high-resolution TEM (HRTEM) image from a 95 nm long region for the (Ga,Fe)As/GaAs structure 180-25. The image demonstrates a smooth homogeneous epitaxial (Ga,Fe)As layer with the thickness of about 45 nm without evident crystalline second-phase inclusions which can usually appear in (III,Fe)V structures in the form of a spherical or oval clusters with a moiré-type contrast [12,13]. The TEM images reveal a large number of stacking faults and microtwins along $\{111\}$ planes, that appear as the assemblage of straight lines at an angle of $\approx 70^\circ$ with respect to each other (Figure 2(a)). The formation of stacking faults and microtwins in epitaxial layers typically is a consequence of the lattice mismatch between an epilayer and a substrate (or a buffer layer) [5,14]. In particular for GaAs layers, similar V-shape stacking defects were observed in the GaAs/Si [15], Ga(As,Bi)/GaAs [16,17] structures and even in the low temperature (LT) GaAs epilayers grown on GaAs substrate (since the lattice parameter of the as-grown LT-GaAs layer is larger than that of the bulk GaAs by 0.1%) [18]. The inset of Figure 2(a) shows a fast Fourier transform (FFT) diffraction pattern of the HRTEM image. The FFT diffraction pattern contains bright primary diffraction spots corresponding to a zinc-blende type lattice of the epitaxial (Ga,Fe)As matrix and additional spots between primary spots. The observation of two additional weak equidistant spots between the pairs of primary spots reveal the presence of additional triple periodicity in the (Ga,Fe)As layer.

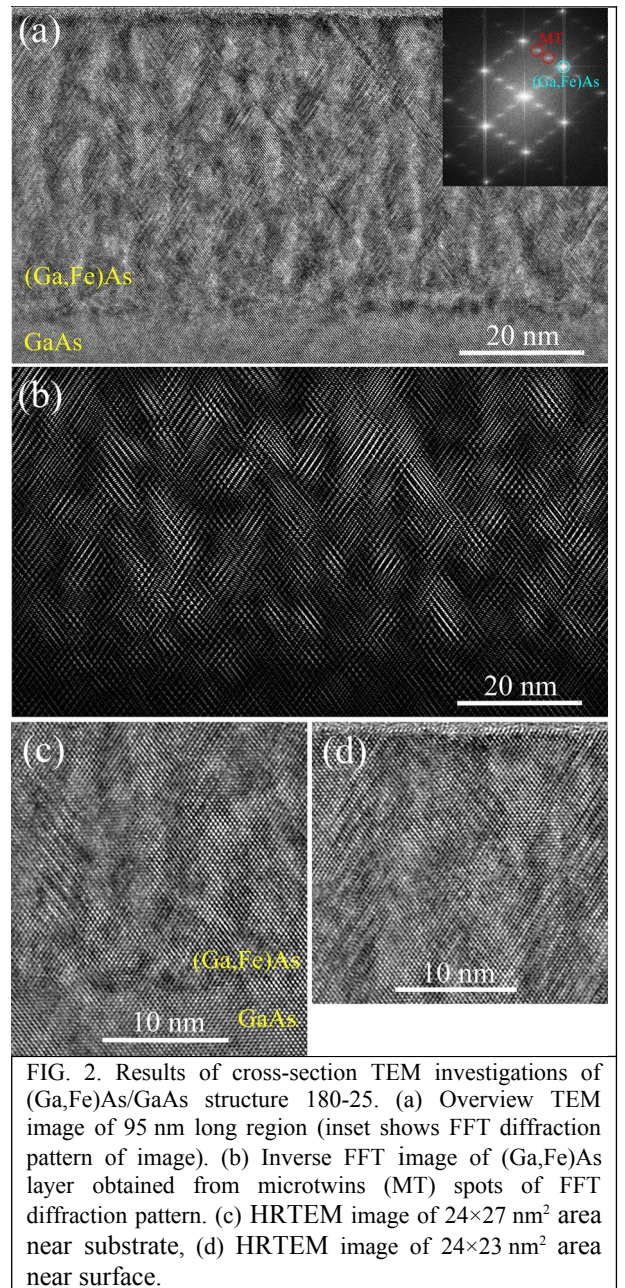


FIG. 2. Results of cross-section TEM investigations of (Ga,Fe)As/GaAs structure 180-25. (a) Overview TEM image of 95 nm long region (inset shows FFT diffraction pattern of image). (b) Inverse FFT image of (Ga,Fe)As layer obtained from microtwins (MT) spots of FFT diffraction pattern. (c) HRTEM image of 24×27 nm² area near substrate, (d) HRTEM image of 24×23 nm² area near surface.

Similar triple periodicity was observed in the GaAs/Si, LT-GaAs/GaAs, Ga(As,Bi)/GaAs structures and was explained by the presence of the regions of the overlapped twins [15-18]. The Figure 2(b) exhibits the inverse FFT image of the (Ga,Fe)As layer obtained from the additional spots of the FFT diffraction pattern. The inverse FFT image reveals, that the regions of the overlapped twins (triple periodicity regions) form periodic columnar-shape domains (Figure 2(b)). For GaSb and InSb matrices the introduction of large number of Fe atoms leads to the lattice constant decrease [1,6]. Since the Fe atomic radius is less than the Ga and As atomic radii, the (Ga,Fe)As lattice constant should also be smaller than the GaAs lattice constant. Apparently this is the cause of the microtwins (and consequently triple periodicity) regions appearance in the obtained (Ga,Fe)As layer. It can be assumed that these regions have the differing lattice constant due to the higher concentration of Fe atoms. In particular,

for the Ga(As,Bi) layers it was observed, that the triple periodicity regions have the higher Bi content [16,17]. The Figures 2(c) and 2(d) show the close-up HRTEM images of the (Ga,Fe)As layer near the GaAs substrate (the $24\times 27\text{ nm}^2$ area, Fig. 2(c)) and near the surface (the $24\times 23\text{ nm}^2$ area, Fig. 2(d)). These HRTEM images confirm the epitaxial growth character of the (Ga,Fe)As layer, the absence of crystalline second-phase inclusions and the presence of the V-shape domains of the microtwins that originate at the (Ga,Fe)As/GaAs interface and propagate further toward the surface.

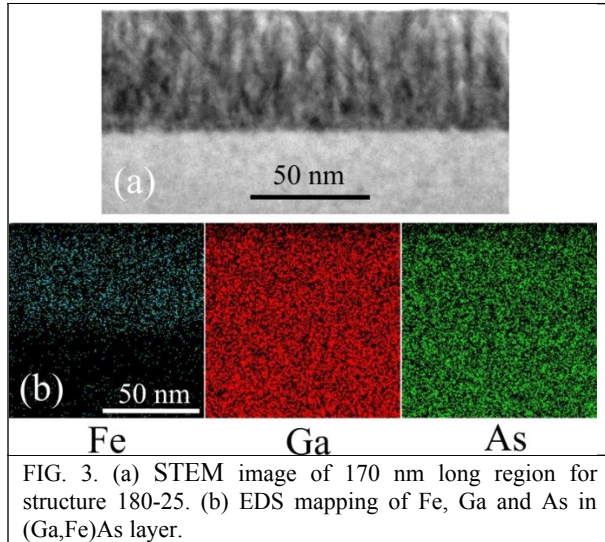


FIG. 3. (a) STEM image of 170 nm long region for structure 180-25. (b) EDS mapping of Fe, Ga and As in (Ga,Fe)As layer.

Figure 3(a) presents a scanning cross-section TEM (STEM) image of the structure 180-25. The STEM image also reveals the presence of periodic columnar-shape structure with the different contrast due to the fluctuations of constituent elements across the periodic columnar domains of overlapped microtwins. The latter can probably be attributed to some fluctuations in the local Fe concentration. The similar structure with the nano-columnar Fe-enriched DMS regions was observed in the 40-nm-thick $(\text{Ga}_{0.7}\text{Fe}_{0.3})\text{Sb}$ layer obtained by MBE on the AlSb buffer layer [4]. Figure 3(b) presents the EDS mapping of Fe, Ga and As atoms for the structure 180-25. The data reveal a rather uniform distribution of the elements within the (Ga,Fe)As layer. The EDS investigations show what the average Fe content in the (Ga,Fe)As layer for the structure 180-25 is about $17\pm 4\text{ at. \%}$. The Fe content (about $20\pm 4\text{ at. \%}$) was also confirmed by X-ray photoelectron spectroscopy.

Figure 4(a) shows the overview HRTEM image from a 73 nm long region for the (Ga,Fe)As/GaAs structure 200-25. As for the structure 180-25 (Fig. 2), the (Ga,Fe)As layer is a smooth homogeneous epitaxial layer with the thickness of about 35 nm without evident crystalline second-phase inclusions. The (Ga,Fe)As layer of the structure 200-25 also contains the regions of the overlapped twins (triple periodicity regions, Fig 4(a) and the inset of Fig. 4(a)). The inverse FFT image of the (Ga,Fe)As layer obtained from the additional spots of the FFT diffraction pattern (the inset of Fig. 4(a)) reveal, that

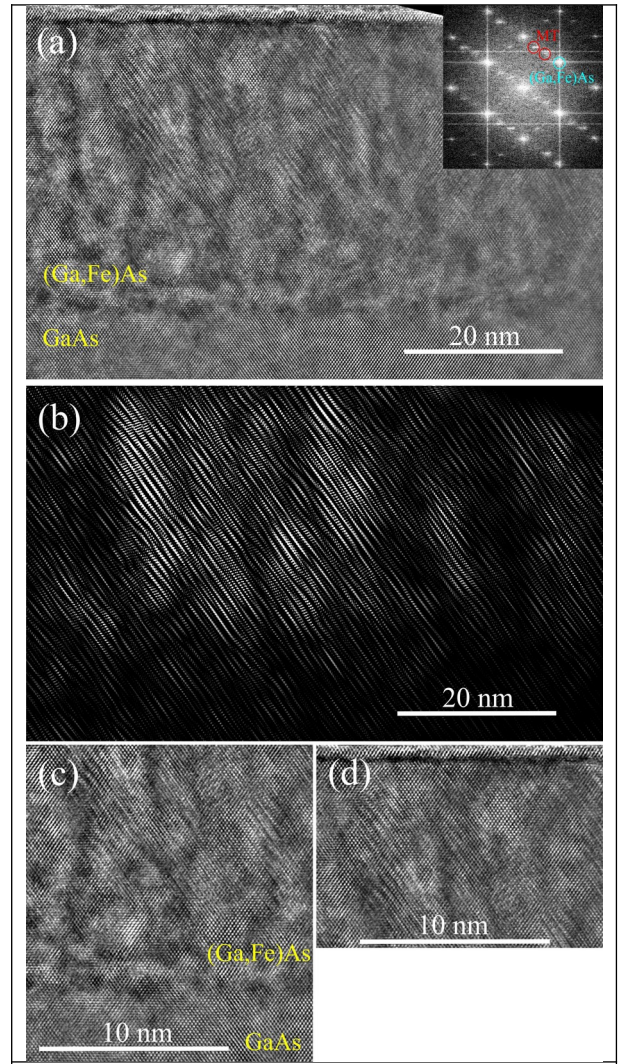


FIG. 4. Results of cross-section TEM investigations of (Ga,Fe)As/GaAs structure 200-25. (a) Overview TEM image of 73 nm long region (inset shows FFT diffraction pattern of image). (b) Inverse FFT image of (Ga,Fe)As layer obtained from microtwins (MT) spots of FFT diffraction pattern. (c) HRTEM image of $15\times 17\text{ nm}^2$ area near substrate, (d) HRTEM image of $15\times 11\text{ nm}^2$ area near surface.

the overlapped microtwins also form columnar-shape domains and these columnar-shape domains are wider (Fig. 4(b)) than that for the structure 180-25 (Fig. 2(b)). The close-up HRTEM images of the $15\times 17\text{ nm}^2$ area near the GaAs substrate (Fig. 4(c)) and of the $15\times 11\text{ nm}^2$ area near the surface (Fig. 4(d)) as for the structure 180-25 (Fig. 2) confirm the epitaxial growth character of the (Ga,Fe)As layer, the absence of crystalline second-phase inclusions and the presence of the domains of microtwins that propagate from the substrate to the surface.

Figure 5(a) presents the STEM image of the structure 200-25. The STEM image confirms the presence of periodic columnar-shape structure with the different contrast, which is again attributed to the some fluctuations of constituent elements including the local Fe concentration. Figure 5(b) presents the EDS mapping of Fe, Ga and As atoms. The data reveal a rather uniform distribution of the elements within the (Ga,Fe)As layer. The EDS investigations

show what the average Fe content in the (Ga,Fe)As layer for the structure 200-25 is about 17 ± 4 at. % as for the structure 180-25. Taking into account this average Fe concentration for the structures 180-25, 200-25 ($Y_{\text{Fe}} = 0.25$) and the technological Fe content for the structures 200-17 ($Y_{\text{Fe}} = 0.17$) and 200-8 ($Y_{\text{Fe}} = 0.08$), the average Fe concentration can be estimated as about 12 and 6 at. % for the structure 200-17 and 200-8, respectively.

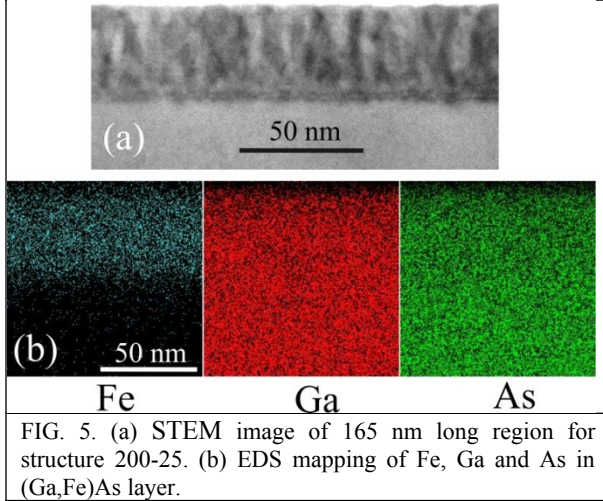


FIG. 5. (a) STEM image of 165 nm long region for structure 200-25. (b) EDS mapping of Fe, Ga and As in (Ga,Fe)As layer.

Although the EDS mapping shows the relatively uniform distribution of Fe within the (Ga,Fe)As layers, however, as indicated above, it is likely that the periodic columnar-shape regions formed by the overlapping twins have the higher Fe concentration than the regions between them. For the structure 200-25 (Fig. 4(b)) these columnar-shape regions are wider and probably have the higher local Fe concentration than for the structure 180-25 (Fig. 2(b)), which can be explained by the faster diffusion of Fe atoms at the higher growth temperature. The presence of columnar Fe-enriched $\text{Ga}_{1-x}\text{Fe}_x\text{As}$ regions separated by $\text{Ga}_{1-x}\text{Fe}_x\text{As}$ regions with a lower Fe concentration should effect the transport and magnetic properties of the obtained layers.

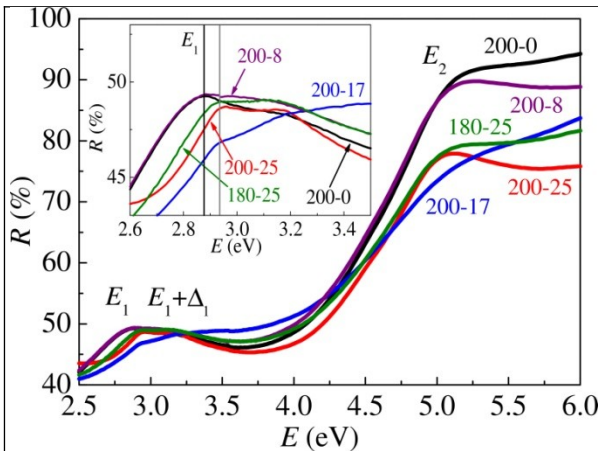


FIG. 6. Optical reflectivity spectra at 295 K for structures 200-0, 200-8, 200-17, 180-25 and 200-25. Inset shows enlarged spectra in E_1 region.

Figure 6 exhibits optical reflectivity spectra at 295 K for the structures 200-0, 200-8, 200-17, 180-25 and 200-25. The reflectivity spectra for the (Ga,Fe)As layers agree with the spectrum for the undoped GaAs layer (the structure 200-0) and contain features associated with characteristic interband transitions for a bulk GaAs [19]. In particular, the doublet in the E_1 region and the intense peak in the E_2 region are observed. This indicates the conservation of the GaAs band structure for the (Ga,Fe)As layers.

For the structures 200-17, 180-25 and 200-25 the E_1 peak has a clear blueshift (the inset to Figure 6). The blueshift of the E_1 peak position with the Fe concentration was observed earlier for the MBE and PLD-grown (Ga,Fe)Sb [13,20] and (In,Fe)Sb layers [6,9].

3.2. Transport and magnetic properties

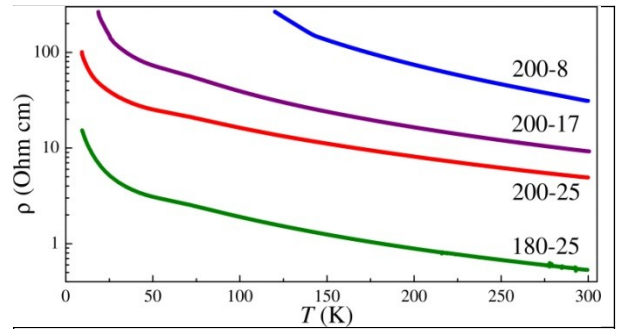


FIG. 7. Temperature dependences of resistivity for structures 200-8, 200-17, 180-25 and 200-25.

Figure 7 shows the temperature dependences of a resistivity $\rho(T)$ for the structures 200-8, 200-17, 180-25 and 200-25. The resistivity of the undoped GaAs layer (the structure 200-0) is high and comparable with the resistivity of the i -GaAs substrate. The $\rho(T)$ dependences are semiconductor type – the resistivity increases with decreasing temperature. The resistivity of the (Ga,Fe)As layers with $T_g = 200^\circ\text{C}$ decrease with the Fe concentration increase. Note that the resistivity value at a given temperature for the structure 180-25 is much lower (about an order of magnitude) than that for the structure 200-25 (Fig. 7).

For the structures 200-8, 200-17, 180-25 and 200-25 the Seebeck coefficient at room temperature corresponds to the n -type conductivity which is consistent with earlier works on the paramagnetic (Ga,Fe)As layers [10-12].

In general, the resistivity of (Ga,Fe)As layers is relatively high. The consequence of this is that the measured Hall resistance dependences on an external magnetic field ($R_{\text{MeasH}}(B)$) are completely determined by the magnetic field dependences of the longitudinal resistivity (magnetoresistance) due to the nonideal Hall measurement geometry of the samples (both for the Hall bars and van der Pauw geometry). For our samples the true Hall resistance dependences on an external magnetic field (an odd function with respect to the B polarity) cannot be correctly extracted from the $R_{\text{MeasH}}(B)$ dependences. The insets of Figures 8(a) and 9(a)

show the $R_{\text{MeasH}}(B)$ curves at 77 and 300 K for the structures 180-25 and 200-25, respectively, for $B = \pm 1.1$ T applied perpendicularly to the sample plane. These are typical $R_{\text{MeasH}}(B)$ dependences for all our (Ga,Fe)As layers. In this connection, we will limit ourselves to the analysis of the magnetoresistance observed in the (Ga,Fe)As layers at different temperatures for the out-of-plane (B is applied perpendicularly to the sample plane) and in-plane (B is applied in the sample plane) orientations.

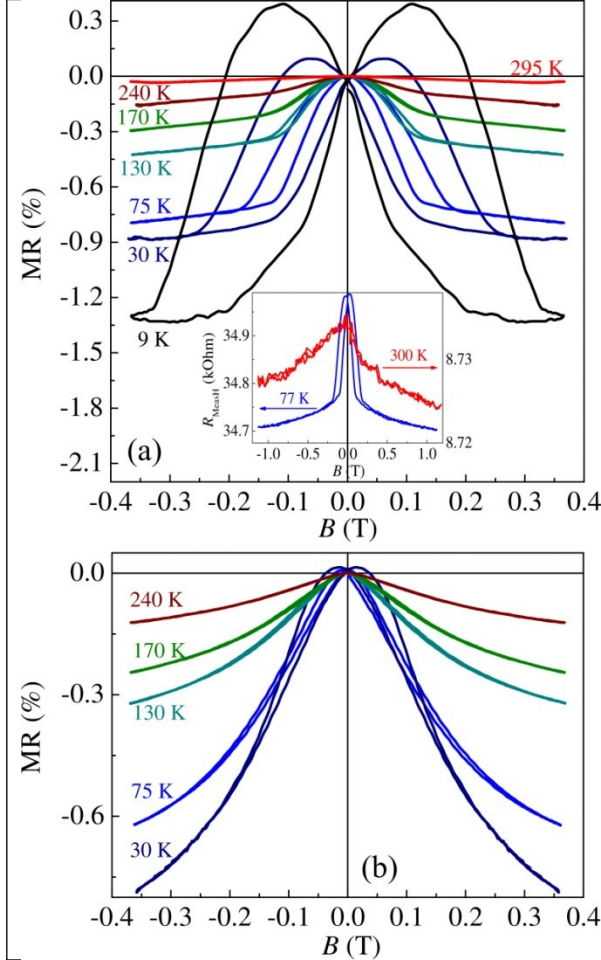


FIG. 8. MR curves at various temperatures for structure 180-25. (a) B is applied perpendicular to sample plane (inset shows $R_{\text{MeasH}}(B)$ curves for $B = \pm 1.1$ T at 77 and 300 K). (b) B is applied in sample plane.

Figure 8(a) shows the magnetoresistance ($\text{MR} = (\rho(B) - \rho(0))/\rho(0)$) curves for the sample 180-25 at temperatures between 9 – 295 K with B applied perpendicular to the plane. A negative hysteretic MR is observed up to 170 K. At 9 K the out-of-plane MR curve has no clear saturation in the magnetic field of ± 0.36 T (the maximum magnetic field available for investigations in the closed-cycle He cryostat). For temperatures above 9 K the out-of-plane MR curves demonstrate the saturation at $B > 0.15 - 0.2$ T (Figure 8(a)). The negative MR with a clear saturation is observed up to 240 K.

Figure 8(b) shows the MR curves for the sample 180-25 at various temperatures with B applied in the plane. For the in-plane orientation the

magnetoresistance is also negative with the hysteretic character up to 170 K. However, the shape of the MR curves at a given temperature are different for the out-of-plane and in-plane orientations. The MR measurements show that at 30 and 75 K the coercivity of the (Ga,Fe)As layer is higher for B applied perpendicular to the sample plane (Fig. 8). Also the MR investigations reveal that the magnetization of the (Ga,Fe)As layer of the structure 180-25 easily saturates when B is applied perpendicular to the sample plane (Fig. 8). These results point to the out-of-plane magnetic anisotropy of the (Ga,Fe)As layer which is apparently related to the presence of the columnar Fe-enriched $\text{Ga}_{1-x}\text{Fe}_x\text{As}$ regions. The similar out-of-plane magnetic anisotropy was observed for the MBE $(\text{Ga}_{0.7}\text{Fe}_{0.3})\text{Sb}$ layers with nano-columnar Fe-enriched DMS regions [4]. The observation of the hysteresis in the magnetoresistance up to 170 K points to the Curie temperature (T_c) about 170 K for the structure 180-25.

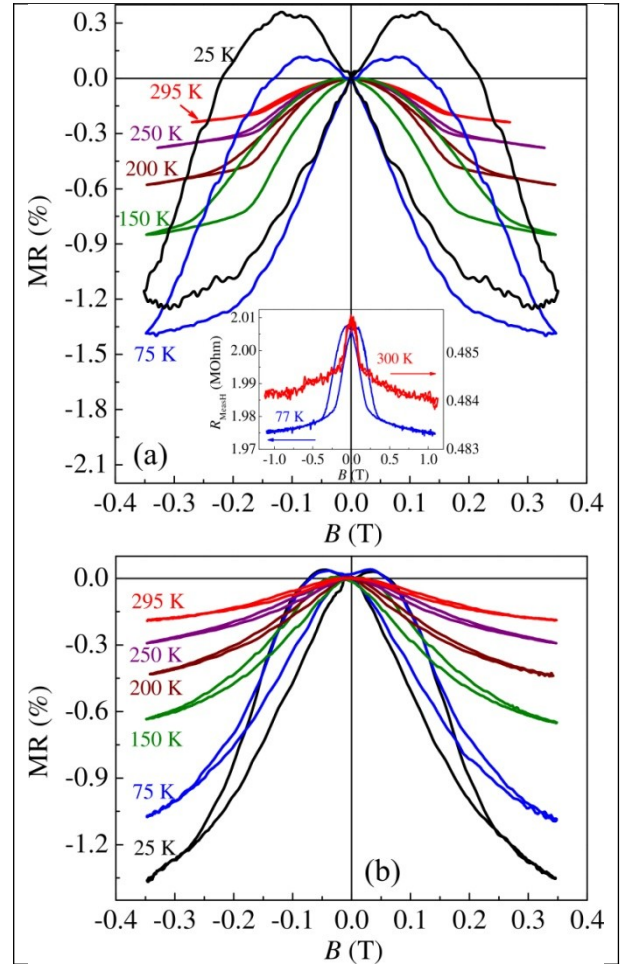


FIG. 9. MR curves at various temperatures for structure 200-25. (a) B is applied perpendicular to sample plane (inset shows $R_{\text{MeasH}}(B)$ curves for $B = \pm 1.1$ T at 77 and 300 K). (b) B is applied in sample plane.

Figure 9 shows the out-of-plane (Fig. 9(a)) and in-plane (Fig. 9(b)) MR curves for the sample 200-25 in the temperature range of 25 – 295 K. For the structure 200-25 the magnetoresistance is negative and hysteretic up to 295 K. A comparison of the out-

of-plane (Fig. 9(a)) and in-plane (Fig. 9(b)) MR curves at the given temperature also points to the out-of-plane magnetic anisotropy of the (Ga,Fe)As layer of the structure 200-25. Inasmuch as the MR curves are hysteretic up to 295 K the T_C for the structure 200-25 is not less than room temperature.

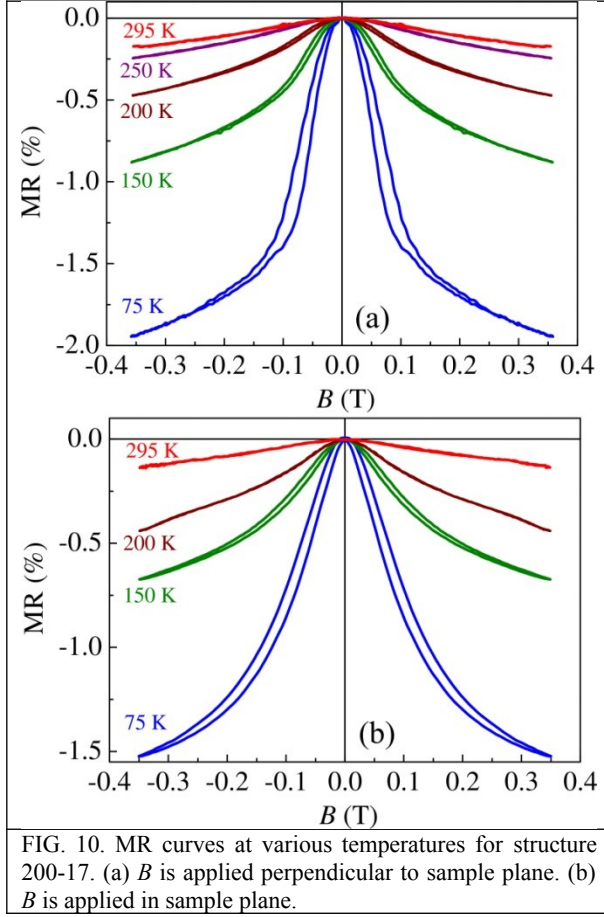


FIG. 10. MR curves at various temperatures for structure 200-17. (a) B is applied perpendicular to sample plane. (b) B is applied in sample plane.

Figure 10(a) shows the MR curves for the sample 200-17 in the temperature range of 75 – 295 K with B applied perpendicular to the plane. As for the structure 200-25 the magnetoresistance is negative up to 295 K but the hysteresis disappears at temperatures above 200 K. The out-of-plane MR curves also show that the coercivity of the (Ga,Fe)As layer for the structure 200-17 is smaller than that for the structure 200-25 (Figure 9) in the all temperature range. The Fe concentration decrease in the structure 200-17 in comparison with the structure 200-25 leads to the weakening of the ferromagnetic properties of the (Ga,Fe)As layer and to T_C reduction. The MR investigations also reveal the out-of-plane magnetic anisotropy of the (Ga,Fe)As layer for the structure 200-17 as for the structures 180-25 and 200-25.

For the structure 200-8 no reliable MR curves were obtained due to the higher resistance of the (Ga,Fe)As layer with the lowest Fe content.

To confirm that the ferromagnetic properties of the obtained layers are related to the intrinsic ferromagnetism of (Ga,Fe)As DMS, the studies of a magnetic circular dichroism were carried out for the structures 180-25 and 200-25. The MCD investigations were performed for B applied

perpendicular to the sample plane. The light from a xenon arc lamp, after passing through a grating monochromator, was circularly polarized by the combination of a linear polarizer and an achromatic quarter-wave plate. This light was incident on the sample surface and reflected from it into the measuring system (photodetector). The MCD value was defined as $((I^+ - I^-)/(I^+ + I^-)) \times 100\%$, where I^+ and I^- are the intensities of circularly polarized light with the right and left circular polarization incident on the sample's surface.

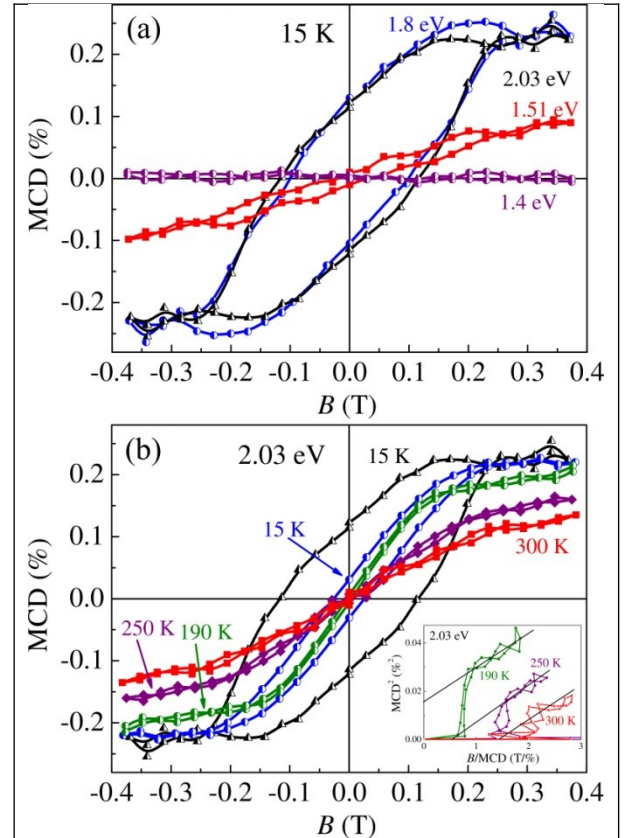


FIG. 11. (a) MCD(B) dependences for structure 180-25 measured for different photon energies at 15 K. (b) MCD(B) dependences for structure 180-25 at different temperatures for photon energy of 2.03 eV. Inset shows Arrhot plot of MCD(B) curves at 190, 250 and 300 K.

Figure 11 shows the MCD dependences on an external magnetic field (MCD(B)) for the structure 180-25 measured at 15 K for the photon energies in the range of 1.4 – 2.03 eV. For the photon energies of 2.03 and 1.8 eV that are notably higher than the GaAs band gap (E_g) at 15 K (~ 1.52 eV), the MCD(B) dependences are hysteretic with the saturation at $B > 0.3$ T and have the maximum amplitude (Fig. 11(a)). When the photon energy decreases to 1.51 eV the amplitude of the MCD(B) dependence drops greatly. For the photon energy of 1.4 eV that is smaller than E_g of GaAs, the detectable MCD value is practically absent (Fig. 11(a)). Figure 11(b) shows the MCD(B) curves for the structure 180-25 for the photon energy of 2.03 eV in the temperature range of 15 – 300 K. The inset of Figure 11(b) shows the Arrhot plot of the MCD(B) curves at 190, 250 and 300 K. The MCD(B) investigations at different temperatures reveal that the

Curie point for the structure 180-25 is about 200 K, this is in agreement with the result of magnetoresistance investigations (Fig. 8).

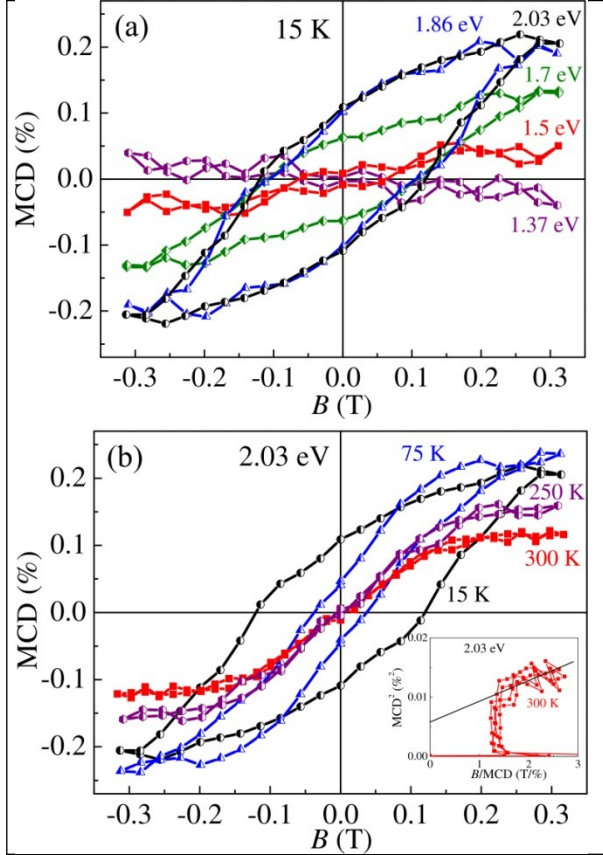


FIG. 12. (a) MCD(B) dependences for structure 200-25 measured for different photon energies at 15 K. (b) MCD(B) dependences for structure 200-25 at different temperatures for photon energy of 2.03 eV. Inset shows Arrort plot of MCD(B) curve at 300 K.

Figure 12(a) exhibits the MCD(B) dependences at 15 K for the structure 200-25 measured for the photon energies in the range of 1.37 – 2.03 eV. While the photon energies are higher than the GaAs band gap, the MCD(B) dependences are hysteretic without the saturation. Note that the hysteretic unsaturated shape of the MCD(B) curves at 15 K is completely consistent with the out-of-plane MR curve at 25 K (Fig. 9(a)). Similarly to as it was observed for the structure 180-25 (Fig. 11(a)), for the photon energy of 1.5 eV that is smaller than E_g of GaAs, the MCD amplitude drops greatly and for the photon energy of 1.37 eV the detectable MCD effect is practically absent (Fig. 12(a)). Figure 12(b) shows the MCD(B) dependences for the structure 200-25 for the photon energy of 2.03 eV in the temperature range of 15 – 300 K. The MCD(B) curves confirm that the (Ga,Fe)As layer of the structure 200-25 is ferromagnetic up to RT (the inset of Fig. 12(b) shows the Arrort plot of the MCD(B) curve at 300 K). The absence of the detectable MCD value for the photon energies ≤ 1.5 eV (when GaAs becomes transparent) reveal that the observed ferromagnetic MCD(B) curves at 15 K (at the photon energies ≥ 1.7 eV) are related to the intrinsic ferromagnetism of the

(Ga,Fe)As layers but not to any second-phase of Fe or intermetallic ferromagnetic inclusions. The spectral dependence of MCD also shows that the E_g of obtained (Ga,Fe)As layers is close to E_g of GaAs. Thus the MCD investigations confirm that the obtained (Ga,Fe)As layers is diluted magnetic semiconductor with intrinsic ferromagnetic properties up to room temperature for the structure 200-25. Since the (Ga,Fe)As layers apparently contain DMS regions with the Fe concentration above average (periodic columnar-shape domains), separated by DMS regions with the Fe concentration below average, these regions have different Curie temperature. The high-temperature intrinsic ferromagnetism evidently is associated with the columnar Fe-enriched DMS regions.

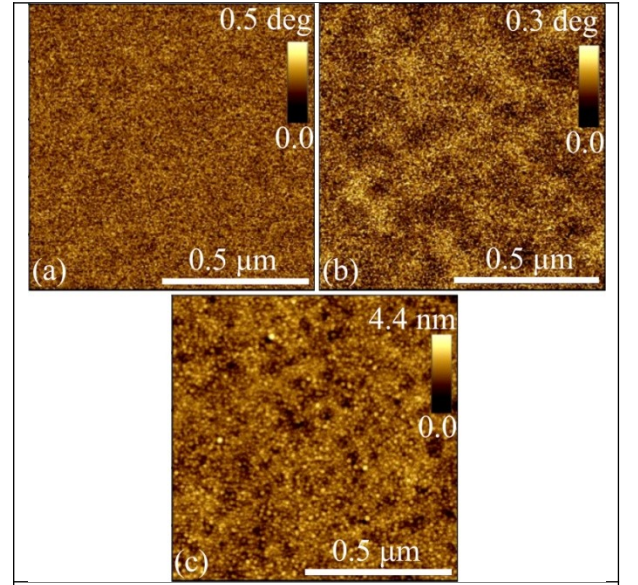


FIG. 13. (a) MFM image for sample 200-25 at $B = 0$. (b) MFM image at $B = 0.23$ T. (c) Corresponding AFM image.

Figures 13(a) and 13(b) show the MFM images obtained at room temperature for the structure 200-25 without an external magnetic field B and with $B = 0.23$ T (applied perpendicular to the plane), respectively. Figure 13(c) shows the corresponding AFM image. The MFM image obtained without an external magnetic field has no magnetic contrast (Fig. 13(a)), however the MFM image at $B = 0.23$ T has a weak but well detectable magnetic contrast (Fig. 13(b)), which clearly differs from the surface morphology of the same part of the structure (Fig. 13(c)). The absence of the magnetic contrast on the MFM image at $B = 0$ apparently related to the small remanent magnetization of the (Ga,Fe)As layers at RT. The observed magnetic contrast at $B = 0.23$ T confirms that T_C for the sample 200-25 is above RT. The results of the MFM studies are consistent with the magnetoresistance and MCD investigations. Note that the surface studies by Kelvin probe force microscopy reveal that the distribution of the surface potential does not coincide with the obtained magnetic contrast, which confirms the correctness of the MFM results. We also note that the control MFM

studies for the structure 200-8 do not reveal any magnetic contrast at $B = 0$ and 0.23 T.

4. Discussion

The fabricated (Ga,Fe)As layers have the rather high resistivity but for the structures 180-25, 200-25 and 200-17 the conductivity is also observed at low temperatures (Fig. 7). This result is interesting in by itself, since the Fe atom forms deep acceptor levels in the GaAs band gap (about 0.88 and 0.51 eV above the valence band (VB) edge [21-25]) and thus should be a compensating impurity. For the Fe atom in the Ga position, two valence s electrons and one d electron participate in the formation of chemical bonds with As atoms [25]. In this case the Fe atom can be in two different valence states: Fe^{3+} ($3d^5$) state - as a neutral impurity (neutral acceptor) and Fe^{2+} ($3d^6$) state - as an ionized deep acceptor [25,26]. It could be expected that the conductivity of the Fe-doped GaAs layers would be comparable to the conductivity of the semi-insulating GaAs. However, it is known, that for the high concentration of an impurity the formation of an impurity band (IB) is possible. In particular, $3d$ elements such as Mn and Ni form the acceptor IB in GaAs [27]. The ferromagnetic properties and the current transfer in the (Ga,Mn)As DMS can be determined by charge carriers in the Mn impurity band separated from VB by a finite energy gap [28-30]. The investigations of the spatial structure of the Fe wave function in GaAs by a scanning tunneling microscopy reveal that the spatial expansion of the Fe wave function is relatively large and can reach 2 – 2.5 nm in different directions [25,31]. In our (Ga,Fe)As layers, the Fe concentration is very high, the Fe local concentration can exceed 20 at. %, i.e. almost 50 % of the Ga atoms are replaced by Fe atoms. In this case the average distance between neighboring Fe atoms is less than spatial expansion of the Fe wave function, which makes it reasonable to assume that the Fe impurity can form the acceptor IB within GaAs band gap. Since Fe is the deep impurity, the formed IB should be separated from the VB. Therefore, the observed transport properties of the obtained (Ga,Fe)As layers are determined by the electron transport in the Fe-related IB. The mobility of the carriers localized within IB should be small (about or less than $1 \text{ cm}^2/\text{V}\cdot\text{s}$). Also, as it was shown by TEM and STEM studies, the periodic vertical structure presumably with some difference in the Fe concentration is observed within the (Ga,Fe)As layers (Figures 2 – 5). This should lead to the spatial inhomogeneity of the impurity band, to the strong modulation of the built-in electric field and consequently to the strong modulation the potential profile. These phenomena should further reduce the carrier mobility, which finally leads to the observed high resistivity of the structures. Taking into account the mobility of about $1 \text{ cm}^2/\text{V}\cdot\text{s}$ and the resistivity of 0.5 Ohm-cm (the resistivity at 300 K for the structure 180-25, Fig. 7), the carrier concentration of an order of magnitude of 10^{19} cm^{-3} can be obtained. This is much lower than

the concentration of introduced Fe atoms. But this is possible, since the Fe acceptor impurity forms the deep (originally empty) acceptor IB in which the charge carriers (electrons) are delivered from some additional donor levels (in particular point defects) and the resulting concentration of electrons participating in the conductivity can be much lower than the acceptor (Fe) concentration. It is most likely that for the structures 200-8, 200-17, and 200-25 the carrier concentration also does not exceed 10^{19} cm^{-3} .

The relatively low carrier concentration indicates that, as in other Fe doped III-V DMSs, the ferromagnetism in the (Ga,Fe)As system is not carrier-mediated. As was mentioned above, the relatively large spatial expansion of the Fe wave function and the high Fe concentration allow the overlapping of the wave functions of neighboring Fe atoms, which permits the direct exchange interaction between Fe atoms. The feature of the (Ga,Fe)As system is also that Fe atoms act as an electrically active impurity and can be in two valence states (Fe^{3+} and Fe^{2+}). Since the nearest Fe atoms are separated by the As atom (with which the Fe atoms have a bond via overlapping the d (Fe) and p (As) shells), the electron transition between Fe^{3+} and Fe^{2+} states is possible, which allows the realization of ferromagnetic ordering via the Zener double exchange mechanism [32]. This mechanism of ferromagnetic exchange interaction in (Ga,Fe)As seems more probable. To determine the mechanism of ferromagnetic exchange (the direct or Zener double exchange) in the (Ga,Fe)As system theoretical studies are necessary. Our presented experimental results definitely show that ferromagnetism (including at RT) may occur in the heavily Fe-doped (Ga,Fe)As layers.

5. Conclusion

In summary, conductive n -type (Ga,Fe)As layers with an average Fe content up to 17 at. % were obtained by the PLD. The TEM and STEM investigations of the (Ga,Fe)As layers with the maximum Fe content revealed that the layer is epitaxial, does not contain any second-phase inclusions, but contains the columnar Fe-enriched regions of overlapped microtwins. These layers can be characterized as a vertical periodic system consisting of nano-columnar regions of a (Ga,Fe)As DMS with an above-average Fe concentration separated by regions of a (Ga,Fe)As DMS with a below-average Fe concentration, similar to what was previously observed for MBE (Ga,Fe)Sb layers [4]. The conductivity of the (Ga,Fe)As layers is apparently associated with the formation of a Fe impurity band within the GaAs band gap. A hysteretic negative magnetoresistance was observed in the layers up to room temperature. Magnetoresistance investigations point to the out-of-plane magnetic anisotropy of the (Ga,Fe)As layers, which is related to the presence of the columnar Fe-enriched $\text{Ga}_{1-x}\text{Fe}_x\text{As}$ regions. The investigations of the magnetic circular dichroism confirm that the layers

are intrinsic ferromagnetic semiconductors with the Curie point up to at least room temperature. It was suggested that in heavily Fe-doped GaAs layers the ferromagnetism is related to the Zener double exchange between Fe atoms with different valence states (Fe^{3+} and Fe^{2+}) via an intermediate As atom. Thus, the possibility of synthesis of conductive (Ga,Fe)As layers with the intrinsic ferromagnetic properties and high Curie temperature has been shown.

Acknowledgements

This study was supported by grant № 18-79-10088 from Russian Science Foundation (except the MFM studies performed M.P. Temiryazeva). N.A Sobolev is gratefully acknowledged for discussion and for the critical reading of the manuscript.

References

1. N. T. Tu, P. N. Hai, L. D. Anh, and M. Tanaka, High-temperature ferromagnetism in heavily Fe-doped ferromagnetic semiconductor (Ga,Fe)Sb, *Appl. Phys. Lett.* **108**, (2016) 192401.
2. Yu. A. Danilov, A. V. Kudrin, V. P. Lesnikov, O. V. Vikhrova, R. N. Kryukov, I. N. Antonov, D. S. Tolkachev, A. V. Alaferdov, Z. E. Kun'kova, M. P. Temiryazev, and A. G. Temiryazev, The study of features of formation and properties of A3B5 semiconductors highly doped with iron, *Phys. Sol. St.* **60**, (2018) 2176–2181.
3. S. Sakamoto, N. T. Tu, Y. Takeda, S. Fujimori, P. N. Hai, L. D. Anh, Y. K. Wakabayashi, G. Shibata, M. Horio, K. Ikeda, Y. Saitoh, H. Yamagami, M. Tanaka, A. Fujimori, Electronic structure of the high- T_C ferromagnetic semiconductor (Ga,Fe)Sb: X-ray magnetic circular dichroism and resonance photoemission spectroscopy studies, *Phys. Rev. B* **100**, (2019) 035204.
4. S. Goel, L. D. Anh, N. T. Tu, S. Ohya, M. Tanaka, In-plane to perpendicular magnetic anisotropy switching in heavily-Fe-doped ferromagnetic semiconductor (Ga,Fe)Sb with high Curie temperature, *Phys. Rev. B* **3**, (2019) 084417.
5. A. V. Kudrin, Yu. A. Danilov, V. P. Lesnikov, M. V. Dorokhin, O. V. Vikhrova, D. A. Pavlov, Yu. V. Usov, I. N. Antonov, R. N. Kriukov, A. V. Alaferdov, and N. A. Sobolev, High-temperature intrinsic ferromagnetism in the (In,Fe)Sb semiconductor, *J. Appl. Phys.* **122**, (2017) 183901.
6. N. T. Tu, P. N. Hai, L. D. Anh, M. Tanaka, High-temperature ferromagnetism in new n-type Fe-doped ferromagnetic semiconductor (In,Fe)Sb, *Appl. Phys. Exp.* **11**, (2018) 063005.
7. L. D. Anh, D. Kaneko, P. N. Hai, and M. Tanaka, Growth and characterization of insulating ferromagnetic semiconductor (Al,Fe)Sb, *Appl. Phys. Lett.* **107**, (2015) 232405.
8. N. T. Tu, P. N. Hai, L. D. Anh, M. Tanaka, Electrical control of ferromagnetism in the n-type ferromagnetic semiconductor (In,Fe)Sb with high Curie temperature, *Appl. Phys. Lett.* **112**, (2018) 122409.
9. A. V. Kudrin, V. P. Lesnikov, Yu. A. Danilov, M. V. Dorokhin, O. V. Vikhrova, D. A. Pavlov, Yu. V. Usov, I. N. Antonov, R. N. Kriukov, S. Yu. Zubkov, D. E. Nikolichev, A. A. Konakov, Yu. A. Dudin, Yu. M. Kuznetsov, M. P. Temiryazeva, N. A. Sobolev, Robustness of ferromagnetism in (In,Fe)Sb diluted magnetic semiconductor to variation of charge carrier concentration, *J. Mag. Mag. Mat.* **485**, (2019) 236–243.
10. S. Haneda, M. Yamaura, Y. Takatani, K. Hara, S. Harigae, H. Munekata, Preparation and Characterization of Fe-Based III-V Diluted Magnetic Semiconductor (Ga, Fe)As, *Jpn. J. Appl. Phys.* **39**, (2000) L9–L12.
11. S. Hirose, M. Yamaura, S. Haneda, K. Hara, H. Munekata, GaFeAs: a diluted magnetic semiconductor grown by molecular beam epitaxy, *Thin Solid Films*, **371**, (2000) 272–277.
12. R. Moriya, Y. Katsumata, Y. Takatani, S. Haneda, T. Kondo, H. Munekata, Preparation and magneto-optical property of highly-resistive (Ga,Fe)As epilayers, *Physica E* **10**, (2001) 224–228.
13. A. V. Kudrina, V. P. Lesnikov, D. A. Pavlov, Yu. V. Usov, Yu. A. Danilov, M. V. Dorokhin, O. V. Vikhrova, V. E. Milin, R. N. Kriukov, Yu. M. Kuznetsov, V. N. Trushin, N. A. Sobolev, Formation of epitaxial *p-i-n* structures on the basis of (In,Fe)Sb and (Ga,Fe)Sb diluted magnetic semiconductors layers, *J. Mag. Mag. Mat.* **487**, (2019) 165321.
14. N. Y. Jin-Phillipp, F. Phillipp, T. Marschner, W. Stolz, E. O. Göbel, Transmission electron microscopy study on defect reduction in GaAs on Si heteroepitaxial layers grown by metalorganic vapor phase epitaxy, *J. Cryst. Growth* **158**, (1996) 28–36.
15. X. J. Wu, F. H. Li and H. Hashimoto, TEM study on overlapped twins in GaAs crystal, *Phil. Mag. B* **63**, (1991), 931-939.
16. M. Wu, E. Luna, J. Puustinen, M. Guina, and A. Trampert, Observation of atomic ordering of triple-period-A and -B type in GaAsBi, *Appl. Phys. Lett.* **105**, (2014), 041602.
17. E. Luna, M. Wu, T. Aoki, M. R. McCartney, J. Puustinen, J. Hilska, M. Guina, D. J. Smith, and A. Trampert, *J. Appl. Phys.* **126**, (2019) 085305.
18. H. Chen, F. H. Li, J. M. Zhou, C. Jiang, X. B. Mei, Y. Huang, Transmission electron microscopy study on GaAs grown by molecular beam epitaxy at low substrate temperature, *J. Mat. Sci. Lett.* **11**, (1992) 1617-1619.
19. R. R. L. Zucca and Y. R. Shen, Wavelength-Modulation Spectra of Some Semiconductors, *Phys. Rev. B* **1**, (1970) 2668.
20. N. T. Tu, P. N. Hai, L. D. Anh, M. Tanaka, Magnetic properties and intrinsic ferromagnetism in (Ga,Fe)Sb ferromagnetic semiconductors, *Phys. Rev. B*, **92**, (2015) 144403.
21. L. A. Hemstreet, Trends in the electronic properties of substitutional 3d transition-metal impurities in GaAs, *Phys. Rev. B*, **22**, (1980) 4590–4599.

22. E. Malguth, A. Hoffmann, M. R. Phillips, Fe in III–V and II–VI semiconductors, *Phys. Stat. Sol. (b)* **245**, (2008) 455–480.
23. J. Bocquel, V. R. Kortan, C. Sahin, R. P. Campion, B. L. Gallagher, M. E. Flatte, and P. M. Koenraad, Core-state manipulation of single Fe impurities in GaAs with a scanning tunneling microscope, *Phys. Rev. B* **87**, (2013) 075421.
24. M. R. Mahani, M. Fhokrul Islam, A. Pertsova, and C. M. Canali, *Phys. Rev. B*, **89**, (2014) 165408.
25. J. Bocquel, V. R. Kortan, R. P. Campion, B. L. Gallagher, M. E. Flatte, and P. M. Koenraad, *Phys. Rev. B* **96**, (2017) 075207.
26. E. M. Omel'yanovskii and V. I. Fistul, *Transition Metal Impurities in Semiconductors* (Adam Hilger Ltd., Bristol, 1983).
27. W. J. Brown Jr., J. S. Blakemore, *Transport and Photoelectrical Properties of Gallium Arsenide Containing Deep Acceptors*, *J. Appl. Phys.* **43**, (1972) 2242.
28. M. Dobrowolska, K. Tivakornsasithorn, X. Liu, J.K. Furdyna, M. Berciu, K.M. Yu, W. Walukiewicz, Controlling the Curie temperature in (Ga, Mn)As through location of the Fermi level within the impurity band, *Nat. Mat.* **11** (2012) 444–449.
29. M. Kobayashi, I. Muneta, Y. Takeda, Y. Harada, A. Fujimori, J. Krempaský, T. Schmitt, S. Ohya, M. Tanaka, M. Oshima, V. N. Strocov, Unveiling the impurity band induced ferromagnetism in the magnetic semiconductor (Ga,Mn)As, *Phys. Rev. B* **89**, (2014) 205204.
30. A.V. Kudrin, O.V. Vikhrova, Yu.A. Danilov, M.V. Dorokhin, I.L. Kalentyeva, A.A. Konakov, V.K. Vasiliev, D.A. Pavlov, Yu.V. Usov, B.N. Zvonkov, The nature of transport and ferromagnetic properties of the GaAs structures with the Mn δ -doped layer, *J. Mag. Mag. Mat.* **478** (2019) 84–90.
31. A. Richardella, D. Kitchen, and A. Yazdani, Mapping the wave function of transition metal acceptor states in the GaAs surface, *Phys. Rev. B* **80**, (2009) 045318.
32. C. Zener, Interaction between the d-Shells in the Transition Metals. II. Ferromagnetic Compounds of Manganese with Perovskite Structure, *Phys. Rev.* **82**, (1951) 403-405.